Am J Physiol Cell Physiol
278: C998–C1010, 2000.

IP_3 receptors, IP_3 transients, and nucleus-associated Ca^{2+} signals in cultured skeletal muscle

ENRIQUE JAIMOVICH,[1,2] ROBERTO REYES,[1]
JOSE L. LIBERONA,[1] AND JEANNE A. POWELL[3]
[1]*Instituto de Ciencias Biomedicas, Facultad de Medicina, Universidad de Chile, Santiago 6530499;*
[2]*Centro de Estudios Científicos de Santiago, Santiago, Chile; and* [3]*Department of Biological Sciences, Smith College, Northampton, Massachusetts 01063*

Jaimovich, Enrique, Roberto Reyes, Jose L. Liberona, and Jeanne A. Powell. IP_3 receptors, IP_3 transients, and nucleus-associated Ca^{2+} signals in cultured skeletal muscle. *Am J Physiol Cell Physiol* 278: C998–C1010, 2000.— Inositol 1,4,5-trisphosphate (IP_3) receptors (IP_3R) and ryanodine receptors (RyR) were localized in cultured rodent muscle fractions by binding of radiolabeled ligands (IP_3 and ryanodine), and IP_3R were visualized in situ by fluorescence immunocytological techniques. Also explored was the effect of K^+ depolarization on IP_3 mass and Ca^{2+} transients studied using a radio-receptor displacement assay and fluorescence imaging of intracellular fluo 3. RyR were located in a microsomal fraction; IP_3R were preferentially found in the nuclear fraction. Fluorescence associated with anti-IP_3R antibody was found in the region of the nuclear envelope and in a striated pattern in the sarcoplasmic areas. An increase in external K^+ affected membrane potential and produced an IP_3 transient. Rat myotubes displayed a fast-propagating Ca^{2+} signal, corresponding to the excitation-contraction coupling transient and a much slower Ca^{2+} wave. Both signals were triggered by high external K^+ and were independent of external Ca^{2+}. Slow waves were associated with cell nuclei and were propagated leaving "glowing" nuclei behind. Different roles are proposed for at least two types of Ca^{2+} release channels, each mediating an intracellular signal in cultured skeletal muscle.

myotubes; inositol 1,4,5-trisphosphate; excitation-contraction coupling; signal transduction

CHANGES IN INTRACELLULAR Ca^{2+} concentration ($[Ca^{2+}]_i$) control a tremendous variety of cell functions, including cell secretion, cell division, and gene expression, such as that associated with cell differentiation (16). In skeletal muscle cells, Ca^{2+} changes are well known to regulate contraction; however, Ca^{2+} changes related to processes other than contraction have received little attention. Nonetheless, we know that at least one pathway might be involved in non-contractile-related Ca^{2+} signaling: the phosphoinositide signaling pathway. The role of the phosphoinositide cycle in the generation of Ca^{2+} signals is well established in many cell types (1). Skeletal muscle fibers possess inositol phosphates, phosphatidylinositol 4-kinase, phosphatidylinositol 4-phosphate-5-kinase, phospholipase C, inositol phosphate phosphatases, inositol 1,4,5-trisphosphate (IP_3) kinase, and G proteins (6–8, 34; for review see Ref. 19). Nevertheless, even though skeletal muscle fibers possess the basic biochemical machinery for the generation and catabolism of inositol phosphates, neither the role nor the regulation of this second messenger pathway has been elucidated in this cell type.

For a clarification of the role of this pathway in skeletal muscle, we need a fuller description of functional correlates of the biochemical evidence. This implies the need for subcellular localization of the Ca^{2+} channels involved as well as characterization of the Ca^{2+} transients related to changes in IP_3 levels. Ca^{2+} transients in cultured muscle are complex, and that complexity may encode the information we seek.

Ca^{2+} release from internal stores may follow more than one set of kinetics and may have more than one function. Ca^{2+} waves have been reported in rodent and chicken myotubes (12, 30). In rat myotubes in vitro, sudden increases in external K^+ concentrations elicit transient elevations in $[Ca^{2+}]_i$ (10, 21). We have used a minimal model involving two components with different kinetics to describe the complex Ca^{2+} release response induced by elevated K^+ (21).

The nucleus is a likely compartment to be involved in Ca^{2+} signaling in muscle cells, since it occupies a large portion of the volume of the myotube. Moreover, evidence for the existence of IP_3 receptor (IP_3R) activity in nuclei of other cell types has accumulated (4, 18, 25, 33, 35). Such activity has been reported to be associated with inner or outer nuclear membranes (1, 14, 27) and to have a role in the control of nucleoplasmic Ca^{2+} concentration, which is associated with gene regulation (5, 22, 26).

To address the question of the existence and possible function of the IP_3 cascade in skeletal muscle, levels of IP_3R and ryanodine receptor (RyR) in nuclear and cytoplasmic fractions of cultured rat muscle were assayed by binding of [^{3}H]IP_3 and [^{3}H]ryanodine. In addition, IP_3R was localized in situ by fluorescence immunocytological techniques. Finally, the effects of K^+ depolarization on IP_3 mass and Ca^{2+} transients were studied using a radio-receptor displacement assay and fluorescence imaging of intracellular fluo 3. We found evidence for a slow $[Ca^{2+}]_i$ transient that is not involved

The costs of publication of this article were defrayed in part by the payment of page charges. The article must therefore be hereby marked "*advertisement*" in accordance with 18 U.S.C. Section 1734 solely to indicate this fact.

in skeletal muscle contraction and evidence for the possible involvement of IP_3R in the generation of that transient in skeletal muscle cells in culture.

METHODS

Animals were handled according to institutional guidelines for animal welfare.

Rat cell cultures. Primary cultures of rat skeletal muscle were prepared as described by Hidalgo et al. (17). Briefly, muscle from the hindlimbs of 12- to 24-h-old rat pups was dissected, and the cells were mechanically dispersed and then treated with 0.2% (wt/vol) collagenase for 15 min at 37°C under mild agitation. The suspension was filtered through Nytex membranes or lens tissue paper and spun down at low speed. After 10–15 min of preplating for enrichment of myoblasts, cells were plated on round coverslips in culture dishes. Densities of $\sim 3.5 \times 10^5$/dish (35 mm) and 9.5×10^5/dish (60 mm) were used for cytosolic Ca^{2+} measurements and IP_3 binding determination, respectively. Plating medium was DMEM-Ham's F-12, 10% bovine serum, 2.5% FCS, 100 mg/l penicillin, 50 mg/l streptomycin, and 2.5 mg/l amphotericin B. To eliminate remaining fibroblasts, 10 μM cytosine arabinoside was added on the 3rd day of culture. After 36 h the medium was replaced with differentiation medium, which is plating medium with a lower concentration of FCS (1.8% vol/vol). Myotubes, some spontaneously contracting, with an estimated purity of >90%, were visible after the 5th day of culture. Most manipulations with rat myotubes were made on 6- to 10-day-old cultures.

Primary mouse cultures and fluorescence immunocytology. Mouse myotubes were grown in culture from enzyme-dissociated newborn hindlimb muscle and processed for immunocytology, as previously reported (13). Cultures were fixed and processed for fluorescence immunocytology at 1–3 wk after fusion of cells into myotubes. Crude and affinity-purified rabbit polyclonal antibodies to type 1 IP_3R, control sera, and synthetic peptide were supplied by Affinity Bioreagents (Golden, CO). The antibodies were raised against a synthetic peptide derived from the COOH-terminal domain of the human type 1 IP_3R peptide. Its sequence was determined from published nucleotide sequences (15): N1829KKKDDEVDRDAPSRKKAKE1848 of the type 1 IP_3R, found in brain and specifically localized in the Purkinje cells of the cerebellum. Cultures were bound with 1:100 and 1:200 dilutions of the whole antibody, 1:25 and 1:50 dilutions of the epitope affinity-purified antibody (1.3 mg/ml), 1:100 and 1:200 dilutions of the preimmune serum, and 1:25 and 1:50 dilutions of the epitope affinity-purified antibody adsorbed with a four times excess (mg/mg) of the peptide.

Ca^{2+} measurements. Intracellular, ionized Ca^{2+} images were obtained from rat myotubes with an inverted confocal microscope (Carl Zeiss Axiovert 135 M, LSM Microsystems). The myotubes were preloaded with fluo 3-AM, which was then deesterified in the cytoplasm. The cells were preincubated in resting solution (see below) containing 5.4 μM fluo 3-AM for 30 min at 25°C. Cells attached to coverslips were mounted in a 1-ml capacity perifusion chamber and placed in the microscope for fluorescence measurements by excitation with a 488-nm-wavelength argon laser beam. Control experiments were performed using an inverted fluorescence microscope (Olympus), and images were acquired with a cooled charge coupled device camera (Spectra-Source MCD 600). A filter wheel (Lambda-10, Sutter Instrument) was used for excitation at different wavelengths; fura 2-AM or microperfused fluo 3 (acid form) was used as a Ca^{2+} dye in this case. The fluorescent images were collected every 0.1–2.0 s and analyzed frame-by-frame with the data acquisition program of the equipment. Cells were incubated in a "resting solution" of the following composition (in mM): 145 NaCl, 5 KCl, 2.6 $CaCl_2$, 1 $MgCl_2$, 10 sodium HEPES, and 5.6 glucose (pH 7.4). Cells were exposed to high-K^+ solutions (47 mM K^+ unless otherwise indicated) and depolarized by a fast (~1 s) change of solution with the perifusion system.

Membrane potential. A number of cells, bathed in resting solution or a high-K^+ solution, were tested to measure the mean membrane potential of a population of myotubes. The whole cell current-clamp method was used, as previously described (23). The intracellular medium contained (in mM) 110 KCl, 1 $CaCl_2$, 1 $MgCl_2$ and 10 HEPES-NaOH (pH 6.9).

Cell fractions and binding of [^{3}H]IP_3 and [^{3}H]ryanodine. For each assay 10–15 culture dishes of 6- to 7-day-old rat myotubes (~3–4 mg cellular protein/dish) were used. Cells were rinsed in PBS plus trypsin-EDTA (0.1% wt/vol) solution for 10–15 min at 28–30°C and then centrifuged at 1,500 *g* for 10 min. The pellet was resuspended in a solution containing 20 mM Tris·HCl (pH 7.5), 1 mM $MgCl_2$, 1 mM dithiothreitol, 150 mM KCl, 100 μM leupeptin, 1 μM pepstatin, and 1 mM phenylmethylsulfonyl fluoride. The cells were homogenized using a Dounce homogenizer ("whole homogenate") and centrifuged at 1,000 *g* for 10 min to obtain a pellet ("crude nuclear fraction"). The supernatant was then centrifuged at 5,000 *g* for 10 min, and this pellet, containing mitochondria and myofibrils, was discarded. The supernatant was centrifuged again at 90,000 *g* for 90 min; the resulting pellet was referred to as the "crude microsomal fraction." Alternatively, the whole homogenate was placed on a discontinuous sucrose gradient (25, 35, and 45% wt/vol sucrose) and centrifuged at 22,000 rpm for 6–8 h in a Beckmann SW 25.1 rotor. Two fractions and the pellet (purified nuclear fraction) of the gradient were washed in a solution that contained 20 mM Tris maleate (pH 7.0) and were centrifuged for 60–80 min at 35,000 rpm in a TFT rotor. Finally, the "purified nuclear fraction" and the 35%-45% interface fraction, the "purified microsomal fraction," were resuspended in 250 mM sucrose plus 20 mM Tris maleate (pH 7.0) and then used fresh or after storage at −20°C for a few days. The purified nuclear fraction was routinely tested for purity and integrity by fluorescence microscopy. After 50 μl of the preparation were incubated with acridine orange (0.125 mg/ml) or Hoe-33342 (1×10^{-3} mg/ml) for 1 min, the preparation was centrifuged at 10,000 rpm for 5 min. The pellet was washed twice with 100 μl of a solution containing 150 mM KCl and 20 mM HEPES·Tris (pH 7.1) and resuspended in 20–30 μl of the same buffer.

The binding of [^{3}H]IP_3 was determined under the following conditions: cell homogenates or cell fractions were incubated at 4°C for 30–40 min in a medium containing 50 mM Tris·HCl (pH 8.4), 1 mM EDTA, and 1 mM β-mercaptoethanol. Different concentrations (from a 1 μM stock) of [^{3}H]IP_3 (D-*myo*-[2-^{3}H]inositol 1,4,5-trisphosphate, specific activity 21.0 Ci/mmol; NEN-Dupont; 800–1,000 cpm/pmol) were added. The reaction was stopped by centrifugation at 10,000 *g* for 10 min (Heraus Biofuge 13), the supernatant was aspirated, and the pellets were washed with PBS and dissolved in 1 M NaOH to measure the radioactivity. The nonspecific binding was determined in the presence of 2 μM IP_3 (Sigma Chemical, St. Louis, MO). [^{3}H]ryanodine binding was measured in rat myotube homogenates and subcellular fractions, as described by Jaimovich et al. (20). The incubation medium contained 0.5 M KCl, 0.1 mM $CaCl_2$, 20 mM HEPES·Tris (pH 7.1), and 1 mM 5′-adenylylimidodiphosphate or 0.5 mM ATP; samples were incubated with [^{3}H]ryanodine (5–100 nM) for 90 min at 37°C in the presence or absence of cold ryanodine (10 μM) for nonspecific binding.

Stimulation of phosphoinositide turnover by high-K^+ depolarization. Rat myotubes were rinsed and preincubated at room temperature for 20 min with the resting solution described above or, to minimize hydrolysis of inositol phosphates, a "high-lithium resting solution" of the following composition (in mM): 58 NaCl, 4.7 KCl, 2.6 $CaCl_2$, 1.2 $MgSO_4$, 0.5 EDTA, 60 LiCl, 5.6 glucose, and 20 HEPES (pH 7.4). Lithium concentration was replaced by equimolar Na^+ when indicated. Next, the cells were stimulated by replacement of this solution with a depolarizing solution of high (47 mM) K^+ with equimolar reduction of NaCl and/or LiCl. In experiments with low external Ca^{2+}, $CaCl_2$ was replaced by equivalent amounts of NaCl, with ion strength in the resting solution kept constant. In some experiments, 0.1 mM EGTA was used instead of EDTA. The corresponding experimental concentrations, determined using a Ca^{2+} electrode, were 61 μM (in EDTA) and 0.17 μM (in EGTA). For the Na^+-free conditions, NaCl was replaced by choline chloride. When the effect of ryanodine was assessed, the cells were preincubated in "resting solution" containing 5–25 μM ryanodine and stimulated with the depolarizing solution in the presence of ryanodine. The reaction was stopped by rapid aspiration of the stimulating solution, addition of 0.8 M ice-cold perchloric acid, and freezing with liquid nitrogen. Cell debris of the thawed samples was spun down for protein determination. The perchloric supernatant was neutralized with 2 M KOH-0.1 M 2-(*N*-morpholino)ethanesulfonic acid-15 mM EDTA. Neutralized extracts were kept frozen until IP_3 quantification.

Radioactive labeling of inositol polyphosphates and separation by anion-exchange Dowex-formiate chromatography. [^{3}H]inositol polyphosphates were obtained from cultures incubated with 2.5 μCi/ml [^{3}H]inositol at 36°C. The soluble perchloric acid extracts containing the [^{3}H]inositol phosphates were neutralized near pH 6.0 with 2 M KOH-0.1 M 2-(*N*-morpholino)ethanesulfonic acid-15 mM EDTA. They were then separated from the potassium perchlorate by centrifugation at 800 *g* for 5 min. The supernatants were applied to a Dowex-formiate column, as described by Downes and Michell (11), and results are expressed as percent experimental level of [^{3}H]inositol phosphates relative to the control level.

IP_3 mass determination. IP_3 mass measurements were carried out as described by Bredt et al. (3). Briefly, a crude rat cerebellum membrane preparation was obtained after homogenization in 50 mM Tris·HCl (pH 7.7), 1 mM EDTA, and 2 mM β-mercaptoethanol and centrifugation at 20,000 *g* for 15 min. This procedure was repeated three times, with the final pellet resuspended in the same solution plus 0.3 M sucrose and frozen at −80°C until use. The membrane preparation was calibrated for IP_3 binding with 1.6 nM [^{3}H]IP_3 and 2–120 nM cold IP_3. The sample analysis was carried out in a similar way, but an aliquot of the neutralized supernatant was added instead of cold IP_3. The [^{3}H]IP_3 radioactivity remaining bound to the membranes was measured by liquid scintillation.

RESULTS

Binding experiments. We studied binding of [^{3}H]ryanodine and [^{3}H]IP_3 to rat myotube homogenates and crude subcellular fractions. A microsomal membrane fraction of 6-day-old myotubes binds ryanodine with a dissociation constant (K_d) of 11.9 ± 0.8 nM and a maximal binding capacity of 1.59 pmol/mg protein (Table 1); a good fit to the equilibrium binding curve implies a single type of receptor (Fig. 1*C*). On the other hand, measurement of [^{3}H]IP_3 binding to crude homogenates of 6-day-old myotubes gave a relatively large binding capacity (4 pmol/mg protein on average) to a single type of receptor (Table 1) with a K_d on the order of 100 nM. Most interestingly, rough subcellular fractionation of the cell homogenates suggests a different subcellular distribution for the two types of receptors (Fig. 1, Table 1). In fact, a fraction enriched in nuclei (1,000-*g* pellet) has little ryanodine binding (0.25 pmol/mg protein) compared with the microsomal membrane fraction (90,000-*g* pellet), which has a 6.4-fold higher concentration of ryanodine receptors (1.59 pmol/mg protein). IP_3 receptors, on the other hand, appear more concentrated in the nuclear fraction, with 11.8 ± 3.2 pmol/plate, compared with 2.4 ± 0.2 pmol/plate in the microsomal fraction (Table 1). The sum of total IP_3 receptors in the microsomal plus the nuclear fraction is less than the total in the homogenate (Table 1); ~40–50% of the receptors were cryptic in membranes forming closed vesicles or lost in the intermediate fraction. Additional measurements were made using a fraction of nuclei obtained after sucrose gradient centrifugation of the cell homogenate. In nuclei that appeared to be intact under the microscope when stained with Hoe-33342 or acridine orange, binding of [^{3}H]IP_3 (2.4 pmol/mg protein, K_d = 92 nM) was not significantly different from that of the cruder nuclear fraction depicted in Table 1. On the other hand, binding of [^{3}H]ryanodine to the purified nuclear fraction was not detectable.

Immunocytochemistry. The type 1 IP_3R complete antibody labels young myotubes very strongly in the nuclear envelope region and some unknown structures

Table 1. *Binding of [^{3}H]IP_3 and [^{3}H]ryanodine in myotube cell fractions*

	[^{3}H]IP_3			[^{3}H]Ryanodine		
Cell Fraction	Binding, pmol/mg protein	K_d, nM	Total Receptors, pmol/plate	Binding, pmol/mg protein	K_d, nM	Total Receptors, pmol/plate
Homogenate	3.9 ± 0.3	110.3 ± 16.1	26.1 ± 3.9	0.87 ± 0.12	25.6 ± 4.2	4.69 ± 0.42
Nuclear	2.7 ± 0.4	89.2 ± 7.9	11.8 ± 3.2	0.25 ± 0.03	15.5 ± 7.5	1.29 ± 0.12
Microsomal	1.7 ± 1.2	92.8 ± 0.6	2.4 ± 0.2	1.59 ± 0.20	11.9 ± 0.8	3.01 ± 0.33

Values are means ± SD obtained from fits to separate curves, each comprising at least 5 points in duplicate, corresponding to 2–4 different membrane preparations. Plates of confluent rat myotubes (6–8 days) were rinsed with PBS, harvested with a rubber policeman, and homogenized with a Dounce homogenizer. Homogenate was centrifuged at 1,000 *g* for 10 min (nuclear fractions), and supernatant was centrifuged at 5,000 *g* for 10 min. Finally, supernatant was centrifuged to >90,000 *g* for 90 min. Resulting pellet was called microsomal fraction. Binding of ^{3}H-labeled inositol 1,4,5-trisphosphate (IP_3) and [^{3}H]ryanodine were measured in all fractions in presence of 2 μM IP_3 and 10 μM ryanodine for nonspecific binding. K_d, dissociation constant.

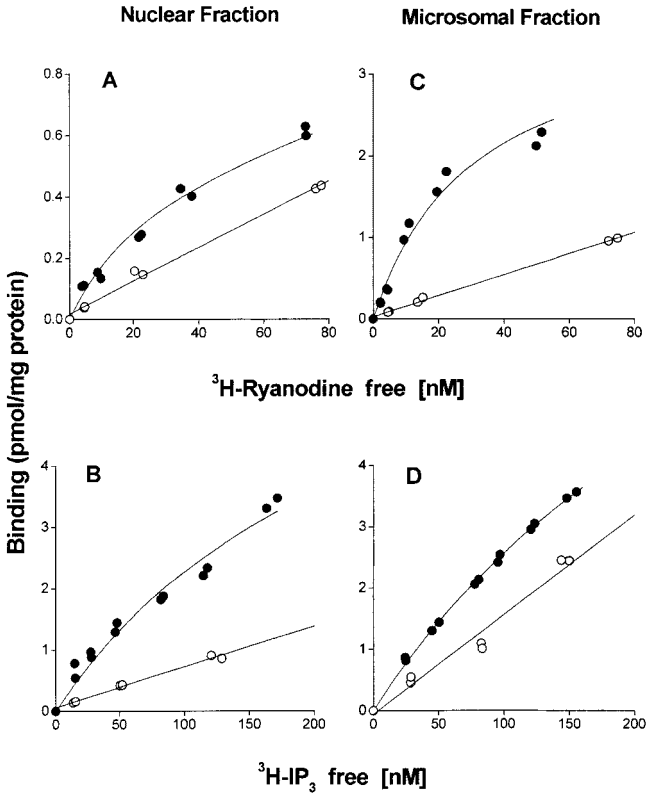

Fig. 1. ^{3}H-labeled ryanodine and inositol 1,4,5-trisphosphate (IP_3) binding to crude subcellular fractions of rat myotubes. *A*: crude nuclear fraction has little [^{3}H]ryanodine binding compared with microsomal membrane fraction (*C*; see also Table 1). A microsomal membrane fraction of 6-day-old myotubes binds ryanodine with a dissociation constant (K_d) of 11.9 ± 0.8 nM and a maximal binding capacity of 1.59 pmol/mg protein; fit to equilibrium binding curve implies a single type of receptor. Microsomal membrane fraction has little [^{3}H]IP_3 binding compared with nuclear fraction (*B;* see also Table 1). Crude nuclear fraction of 6-day-old myotubes gives a large binding capacity, ~4 pmol/mg protein, compared with microsomal membrane fraction (*D*). [^{3}H]IP_3 binding to crude nuclear fraction shows a single type of receptor with K_d = 89.2 nM. Total binding (●) and nonspecific binding (○) measured in presence of 10 μM ryanodine or 2 μM IP_3 are shown; for estimation of specific binding, straight line (correlation coefficient >0.95 in all cases) was subtracted from curve at each point.

within the nucleus at dilutions of 1:100 and 1:200. The same labeling pattern was seen when epitope affinity-purified antibody solutions (at dilutions of 1:25 and 1:50) were bound to the cultures (Fig. 2*A*). The internal nuclear staining is not specific for the IP_3R, since the preimmune serum also binds the internal structures (Fig. 2*B*). The affinity-purified antibody binds also to mature cross-striated myotubes that show, in addition to nuclear staining, a cross-striated IP_3R stain (Fig. 2*E*). Mouse and rat (not shown) myotubes stained similarly. The "nuclear envelope" and cross-striated cytoplasmic stain were completely eliminated when the IP_3R affinity antibody was adsorbed with the specific peptide used to raise the antibody (Fig. 2*C*, *bottom*). In the present study we labeled Purkinje cells cultured from 14–day embryonic cerebella with the same complete antibody to the type 1 IP_3R, and these cells lit up uniformly throughout the cell body and dendrites, as expected (data not shown).

Cytosolic levels of IP_3. The absolute resting mass of IP_3 varied between independent cultures plated at different times, and sometimes it was necessary to normalize the results from independent experiments by indicating the change in IP_3 mass relative to basal levels. This allowed us to compare the changes induced by the different stimuli. A study performed in 60 dishes from 21 independent primary cultures yielded a mean IP_3 resting mass of 28.4 ± 10.6 pmol/mg cell protein, with individual cultures ranging from 9 to 50 pmol/mg cell protein. Although culture conditions were kept constant, differences between individual cultures could be partly attributed to slightly different maturation conditions. From these 21 primary cultures, 18 (85%) responded with a significant net increase of IP_3 on K^+ depolarization (see below).

Effect of K^+ depolarization on the IP_3 levels. A 2- to 4-s exposure to increasing external K^+ concentrations positively affected IP_3 levels in rat myotubes in primary culture (Fig. 3, *inset*). When extracellular K^+ concentration was 4.7 mM, measured resting membrane potential (V_m) was −41 ± 6 mV (n = 28 cells). The dose-response relationship between external K^+ concentration and IP_3 (Fig. 3, *inset*) was arbitrarily fitted to a sigmoidal curve that is roughly similar to that described by Jaimovich and Rojas (21) for the relationship between external K^+ concentration and the peak of the $[Ca^{2+}]_i$ concentration in these cells. In the present experiment, the minimum external K^+ concentration needed to affect a change in IP_3 mass was 22 mM (measured V_m = −26 ± 5 mV, n = 3 cells), and the maximum was near 47 mM external K^+ (measured V_m = −12 ± 4 mV, n = 10 cells). Further increases in K^+ concentration did not produce higher levels of IP_3, even when applications of external K^+ as high as 63 and 83 mM continued to depolarize the myotubes to −6 and +1 mV, respectively.

Time course of the K^+-induced IP_3 increase and effect of external Ca^{2+}. The effect of 47 mM K^+ depolarization on the IP_3 level at different times is depicted in Fig. 3. K^+ induced a three- to fourfold transient increase on the IP_3 mass visible after 2 s of stimulation or after 10–15 s. There is a transient drop in IP_3 mass levels between 2 and 5 s in rat myotubes in primary culture under standard conditions (Fig. 3), but a detailed study of the first part of the curve was not possible, since 2 s is the time resolution limit of our experimental system. The level of IP_3 was still significantly higher than basal after 60 s of depolarization, whereas there was no significant difference from the control condition 6 min after K^+ stimulation. The effect of K^+ was still visible in the absence of externally added Ca^{2+}. The replacement of the bathing solution with Na^+-free, Ca^{2+}-free medium (made by substitution of external Na^+ by choline and EGTA addition) did not alter the effect of K^+ (Fig. 4*A*), nor did reduction of external lithium from 60 mM to 20 or 0 mM (not shown). Thus any influx of cations such as Ca^{2+} or Na^+ could be dismissed as a requirement for increasing IP_3 mass.

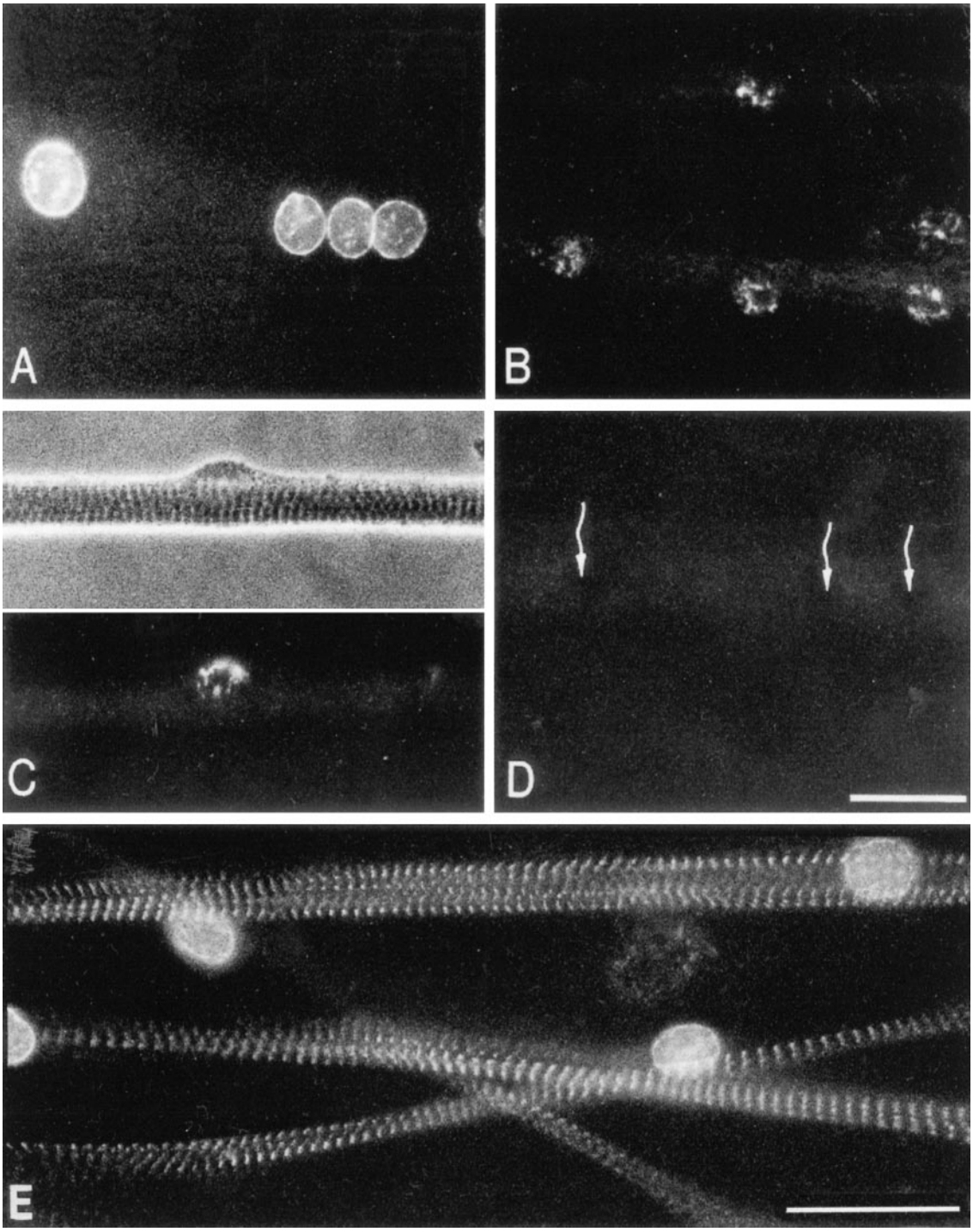

Fig. 2. Fluorescence immunolabeling of type 1 IP_3 receptors (IP_3R). *A*: epitope affinity-purified rabbit polyclonal antibody to IP_3R labels nuclear envelope region and some internal nuclear structures; latter label is nonspecific, since preimmune serum (*B*) labels only internal nuclear structures, here seen in 2 myotubes; nuclear envelope region is not labeled. *C*: internal nuclear labeling is nonspecific, as shown in well-differentiated myotube (*top*) in phase-contrast optics; *bottom*: same field labeled with IP_3R epitope affinity-purified antibody, adsorbed with 4 times excess (mg/mg) of epitope peptide. *D*: myotubes show very faint fluorescence when incubated with fluorescence-conjugated secondary antibody alone. Black unstained nuclei can barely be seen (arrows). Scale bar in *D* for *A–D*, 30 μm. *E*: mature, differentiated myotubes labeled with IP_3R epitope affinity-purified antibody. Nuclear envelope and cytoplasmic regions are positively labeled. Label in cytoplasm is found in a cross-striated pattern and is specific for IP_3R, since same type of myotube in *C* is a negative control and shows no staining in cross-striated tube shown in phase. Scale bar, 30 μm.

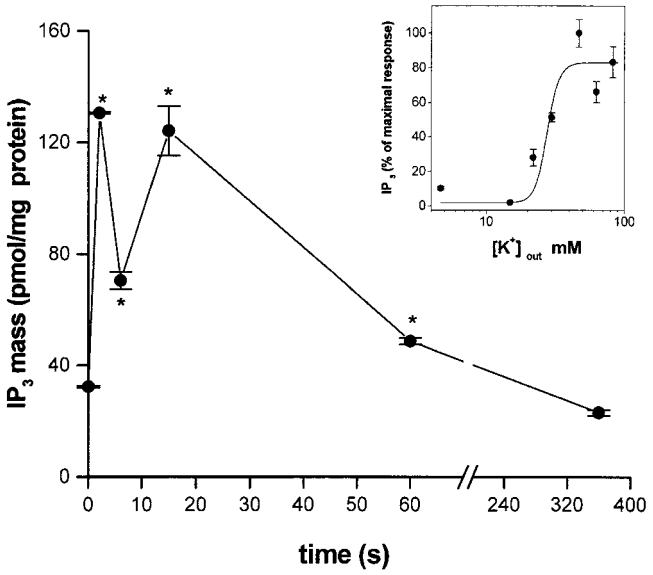

Fig. 3. Effect of changes in external K^+ concentration ($[K^+]_{out}$) on IP_3 mass. *Inset*: IP_3 mass changes in different external K^+ concentrations. Seven-day-old myotubes were preincubated for 20 min in resting solution and then depolarized with different concentrations of K^+. Reaction was stopped at 4 s with 0.8 M perchloric acid, and neutralized extract was tested by radio-receptor assay for IP_3. Maximally stimulated over basal values were 3.6 ± 0.3 in 15 experiments from 7 different cultures. Standard stimulation was performed with 47 mM K^+. Values are means ± SD from 2 independent experiments performed in triplicate. Time course of IP_3 mass changes on K^+ depolarization in rat skeletal muscle primary cultures is shown in 7-day-old myotubes preincubated for 20 min in resting solution and then depolarized with 47 mM K^+. IP_3 mass was measured in soluble extract. Values are means ± SD from 3 independent experiments performed in triplicate. $^*P < 0.001$ vs. basal (Student's paired *t*-test).

Influence of $[Ca^{2+}]_i$ release on the K^+-induced IP_3 increase. Although an early K^+-elicited IP_3 rise is visible in the absence of external Ca^{2+}, hypothetically the IP_3 rise could be mediated by $[Ca^{2+}]_i$ release. We negated this possibility using ryanodine to block fast release of Ca^{2+} from internal stores. The observation of K^+-induced IP_3 mass increase in rat myotubes, incubated with ryanodine (Fig. 4*B*), suggests that a significant part of the K^+-induced stimulation of phosphoinositide turnover is independent of release of Ca^{2+} from the sarcoplasmic reticulum (SR; see below). We must conclude then that a separate mechanism, probably triggered by membrane depolarization, influences IP_3 generation.

Precursors and metabolites of IP_3. An increase in the mass of IP_3 can be attained by an increase in the rate of synthesis or a reduction in degradation. We performed measurements using cells preincubated with tritiated inositol to study label incorporation into various phosphoinositides and inositol phosphates. Radioactivity in the lipid phase increased on K^+ depolarization, and significant differences in ^{3}H-labeled phosphatidylinositol 4,5-bisphosphate (PIP_2) values with respect to basal levels were found after 5 s in high K^+ (Fig. 4*C*). Radioactivity in PIP_2 tends to decrease after 60 s. Values of phosphatidylinositol 4-phosphate and phosphatidylinositol increased (not shown) less than PIP_2. On the other hand, measurements of tritiated inositol

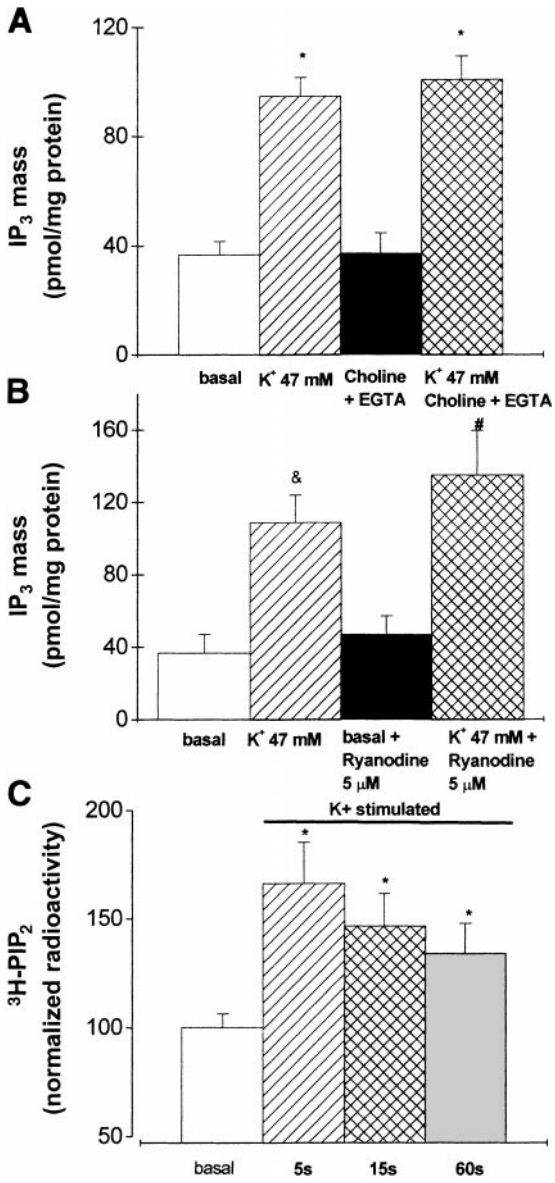

Fig. 4. *A*: IP_3 mass changes on K^+ depolarization in rat skeletal muscle primary cultures. Effect of external Ca^{2+} and Na^+ is shown in 7-day-old myotubes preincubated for 20 min in resting solution containing 20 mM lithium and then depolarized with 47 mM K^+ in presence or absence of Ca^{2+} and Na^+ (EGTA and choline substitution) in incubation medium. IP_3 mass was measured in soluble extract. Values are means ± SD from 3 independent experiments performed in triplicate. $^*P < 0.001$ vs. basal (Student's paired *t*-test). *B*: IP_3 mass changes on K^+ depolarization in rat skeletal muscle primary cultures. Effect of ryanodine is shown in 7-day-old myotubes preincubated for 10 min in resting solution (with or without 5 μM ryanodine) and then for 2 min in resting solution containing EGTA in absence of Ca^{2+} (with or without 5 μM ryanodine). Then they were incubated for 4 s in a similar solution containing 47 mM K^+ (see Fig. 3). Values are means ± SD from 3 independent experiments. $^{\&}P < 0.01$; $^{\#}P < 0.05$ vs. basal (Student's paired *t*-test). *C*: ^{3}H-labeled phosphatidylinositol 4,5-bisphosphate (PIP_2) changes on K^+ depolarization in rat skeletal muscle primary culture. Seven-day-old myotubes were preincubated for 20 min in resting solution and then depolarized with K^+ during different time periods. [^{3}H]PIP_2 was measured in soluble extracts after Dowex-formiate chromatography. Values are means ± SD from 3 independent experiments in triplicate. $^*P < 0.001$ vs. basal (Student's paired *t*-test).

phosphates (not shown) indicated significant increases in IP_3 and inositol bisphosphate, with little effect on the levels of inositol phosphate under the conditions used. These results suggest an effect of K^+ depolarization on the rate of inositide lipid phosphorylation.

Ca^{2+} imaging. Confocal microscopy was used to study fluo 3 fluorescence in rat myotubes in primary culture after stimulation by the addition of high extracellular K^+ under various conditions. Confocal microscopy allowed us to image one fast and one or more slow intracellular fluorescence rises. The time resolution of our system does not allow us to follow the detailed evolution of the fast signal, but we were often able to see part of it. In a typical experiment (Fig. 5*A*), a fluorescence rise that spans the whole cell and lasts <1 s can be seen immediately after K^+ was increased. Seconds after the fast signal faded, a focus of fluorescence appeared in the *extreme right* of the myotube (Fig. 5*B*, 3.60–4.20 s). The slow propagation of a Ca^{2+} wave became evident during and after this period (Fig. 5, *B* and *C*, 3.60–8.70 s; note different time scales). The slow signal can be envisaged as having two components: a more rapid, more diffuse component (the "slow-rapid component") of low fluorescence (green-blue) that always precedes a localized, high-fluorescence (yellow-red) wave (the "slow-slow" component; Fig. 5*C*). As fluorescence progressed, the presence of high-fluorescence spots, usually identifiable with cell nuclei (Fig. 5*C*), became evident. We believe that the high-fluorescence spots are due to fluo 3 signal from inside the nucleus rather than from the perinuclear cytoplasm. As stated above (see also the bright-field image in Fig. 5, *A*–*C*), the spots correlate in space with the position of nuclei.

Control experiments were performed to test whether an inhomogeneous distribution of fluo 3 could be respon-

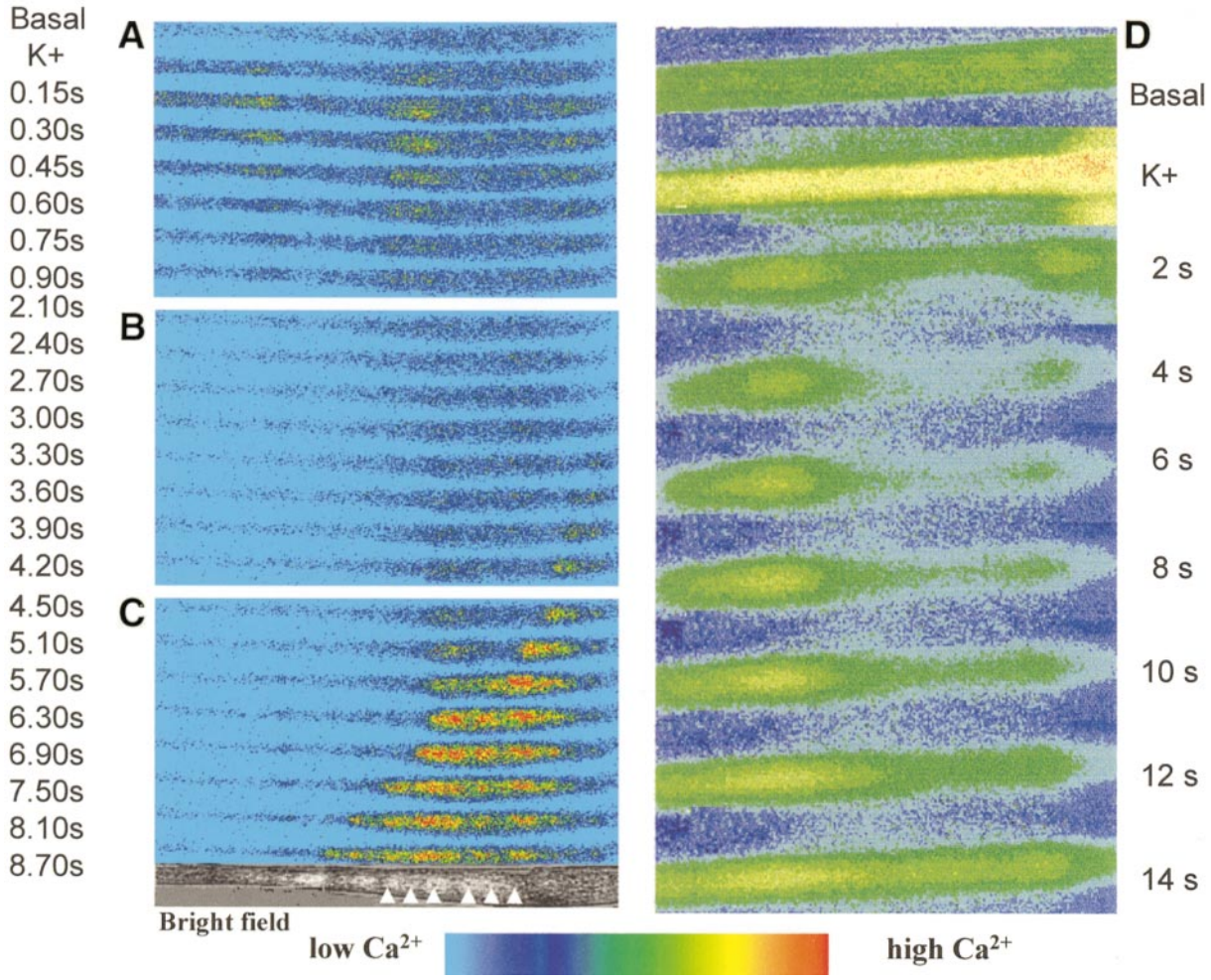

Fig. 5. Ca^{2+} images of fluo 3 fluorescence by confocal microscopy (*A*–*C*) and fura 2 fluorescence ratio (*D*) in a rat myotube. Confocal imaging allowed dissection of a fast and a slow intracellular Ca^{2+} concentration ($[Ca^{2+}]_i$) rise. Basal fluorescence is shown at *top* of *A*. Next image was taken immediately after bath solution was quickly changed to 47 mM K^+; this solution remained in bath throughout record. Subsequent images were taken every 150 ms (*A*). After fast signal faded, images in *B* were taken every 300 ms. A focus of fluorescence appears in *extreme left* of myotube (*B*, 3.6–4.2 s), and slow propagation of a Ca^{2+} wave becomes evident (*C*). Images in *C* were taken every 600 ms. Fluorescence is higher in confined regions, where nuclei are found (*C*). Nuclei are pointed out in bright-field plus fluorescence image of this cell (*bottom* of *C*). Total length of myotube section is 354 μm. Image ratios of a fura 2-loaded cell were taken every 2 s (*D*) stimulated (K^+) as in *A*. Total length of myotube section is 225 μm.

sible for apparent differences in Ca^{2+} concentration within the cell. The ratiometric dye fura 2 allowed us to evaluate the relative changes in free Ca^{2+} concentrations produced during fast and slow responses to high K^+. In ratio images taken every 2 s (Fig. 5*D*), $[Ca^{2+}]_i$ increased immediately on high-K^+ perifusion (Fig. 5*D* is representative of 8 independent experiments); a substantial decrease in $[Ca^{2+}]_i$ follows (2–4 s), and a slow, propagated rise in $[Ca^{2+}]_i$ was evident between 6 and 14 s. The ratio of fluorescence was clearly nonhomogeneous during the slow wave, higher Ca^{2+} levels being concentrated in the central part of the myotube, as in Fig. 5*C*. It was also evident that cytosolic Ca^{2+} concentration is much higher during the fast response. A total of 84 independent experiments with high K^+ and fluo 3 were recorded; mouse (not shown) and rat myotubes behaved similarly. The slow rise in fluo 3 fluorescence described here was evident in 75 records (89%). The fast fluorescence transient was not always evident, possibly because of the limited time resolution (0.5–1 images/s in many cases). When relatively fast (100–400 ms/image) acquisition protocols were used, the fast signal was present in 18 of 19 experiments recorded. In our experimental conditions, ≥100 ms were needed to acquire an image of a significant part of a myotube. The rate of solution change was a critical factor in producing slow (and fast) transients. If the rate of replacement of the resting solution by the high-K^+ medium was too slow, it often failed to produce a measurable fluorescence signal, possibly because of inactivation of the voltage sensor. A flux of ≥0.5 ml/s was needed to see Ca^{2+} changes. The cell diameter was monitored in bright-field images before and after solution changes; no cell swelling was observed as a result of osmotic imbalance after isosmotic high K^+ concentration was applied. Nonetheless, in conditions in which cell shrinkage was evident (experiments where hyperosmotic KCl concentration was achieved by addition of 10–20 μl of 1 M KCl to a final concentration of 20–30 mM), exactly the same type of fluorescence signals were seen, indicating that shrinkage has no effect.

Contraction is not a factor in affecting the signal intensity in the sarcoplasm. The two types of Ca^{2+} signals were seen in mature myotubes (capable of contraction) and young, immature myotubes (incapable of contraction). The fast, early Ca^{2+} transient was usually associated with a contracture in mature myotubes and, thus, reflected an excitation-contraction (E-C) coupling event. However, the slow propagated Ca^{2+} signals were not associated with contraction of the myotube. Lack of contraction during the slow wave is illustrated in Fig. 6, *left*, in which a series of fluorescence images were superimposed on the bright-field image of the myotube, acquired before K^+ stimulation (Fig. 6, *top left*). Propagation and collision of two slow Ca^{2+} waves can be seen, whereas no displacement of the fluorescent image, with respect to the original bright-field image, was observed. Moreover, differences in the bright-field image between regions that propagated the wave and those that did not were not evident. Thus we conclude that changes in intensity reflect changes in $[Ca^{2+}]_i$, not changes in cell geometry.

Other interesting aspects of the slow wave are illustrated in Fig. 6, *left*. For example, propagation of the waves appears limited to a portion of the myotube. Also as illustrated, propagation of the slow wave often stops at a certain spot. Finally, when two waves collide (Fig. 6, *left*), they tend to annihilate (not shown) and do not progress further to regions where fluorescence was recently high.

Figure 6, *right*, illustrates the difference between nuclear and cytoplasmic slow fluorescence signals. The relatively low fluorescence elicited by this wave allows us to see that the fluorescence signal is much brighter in the cell nuclei than in the cytosol and that it propagates in sequence, from one nucleus to another. By cycling between high-K^+ and resting medium, we could usually elicit several high-K^+-stimulated Ca^{2+} waves. One of these slow waves is shown in Fig. 6, *right*. Figure 6, *right*, shows the result when high-K^+ medium was added after two previous waves had already been elicited and the corresponding high-K^+ solutions were replaced by resting medium. Local propagation is easier to see in regions where neighboring nuclei are close, but an increase in fluorescence propagates as well (and apparently faster, see below) through regions seemingly devoid of nuclei.

A careful analysis of the Ca^{2+} signals shows several important points concerning the characteristics of the fast and slow Ca^{2+} waves. The fast Ca^{2+} signal develops during the 1st s in the cytoplasm and nuclear regions. In Fig. 7*A*, the relative changes in fluorescence of three different areas of a cell are displayed as a function of time. The fast Ca^{2+} signal develops in all three spots during the 1st s; also, the relative change in fluorescence is higher (and lasts longer) in the cytosol than in the nuclei. Several seconds after the fast fluorescent change is over, a large relative change in fluorescence is evident (a slow wave moving from right to left). This slow wave exhibited characteristics that contrast with those of the fast wave: the relative change in cytoplasmic fluorescence was much less in this later wave than in the nuclei.

Figure 7 also provides information about the propagation time of the slow wave. The time shift between the two nuclear signals implies an apparent mean propagation velocity for this wave of 48 μm/s. When we compare the propagation of the slow wave in cytosolic regions with that in regions containing rows of nuclei (Fig. 7*B*), differences become apparent. By choosing two areas of identical projected surface, located 34 μm apart in a region of the cell devoid of active nuclei, the relative changes in fluorescence in each area occur stepwise (Fig. 7*B*, open symbols). The shift between the two signals allows us to calculate a propagation velocity for the wave of ~70 μm/s. The procedure was repeated using two spots separated by the same distance in a region where a row of nuclei was apparent (Fig. 7*B*, filled symbols); more complex kinetics were displayed. The propagation velocity was different depending on how we defined the wave front. If we consider the front

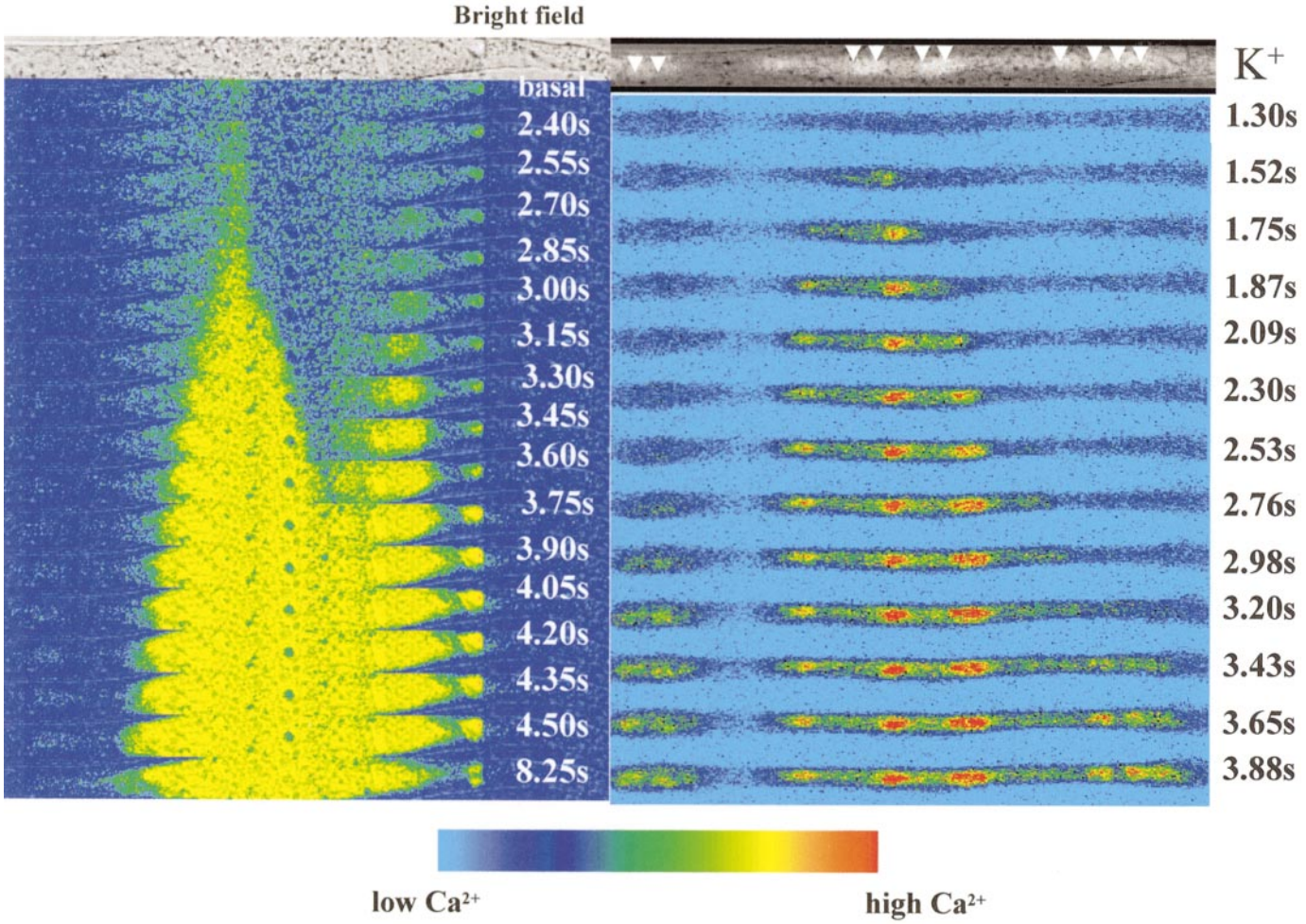

Fig. 6. *Left*: slow propagated Ca^{2+} wave is not associated with contraction of myotube. Each of a series of fluorescence images (taken every 150 ms) was superimposed on same transmitted light image of myotube (bright field), acquired before K^+. Propagation and collision of 2 slow Ca^{2+} waves can be seen, and no displacement of fluorescent image with respect to transmitted image was observed. Total length of myotube section is 314 μm. *Right*: high-K^+ medium was added after 2 previous waves were elicited, and corresponding high-K^+ solutions were replaced by normal medium. Relatively low fluorescence elicited by this slow wave allows us to see that Ca^{2+} signal is mainly located in cell nuclei and that it is propagated in sequence, from one nucleus to another. Total length of myotube section is 243 μm.

to be the initial, low-fluorescence rise, a speed of ~70 μm/s will be obtained. In contrast, if we consider the time at 80% maximal fluorescence, a propagation velocity on the order of 20 μm/s will be estimated. We believe that in some cells (not shown) the fluorescence signal was so faint that all we could see was a "nuclear" wave propagating at speeds of 10–25 μm/s. Thus we used the maximal fluorescence to estimate propagation velocity for the nuclear wave. The mean propagation velocity for this type of signal was 16 ± 6 μm/s (n = 6), whereas the cytosolic slow wave had a propagation speed of 56 ± 9 μm/s (n = 9). Therefore, we called the nuclear wave the slow-slow wave and the cytosolic wave the rapid-slow wave.

We do not know whether fluo 3 distributes homogeneously between the cytosol and nuclear compartments. Because of this possible inhomogeneity, we were not able to quantify the absolute values of Ca^{2+} concentration in the nuclear or the cytosol compartments. We can state, however, that for the slow Ca^{2+} wave the ratio of fluorescence relative to basal values increases more in the nucleus than in the rest of the cell, and this increase reaches its peak after the cytosol (Fig. 7*B*).

To test for a possible component of Ca^{2+} influx in these signals, a total of 11 experiments were performed in the absence of external Ca^{2+}, with 0.5 mM EGTA in the incubation media. The fast Ca^{2+} transient and the slow Ca^{2+} wave were clearly present in this condition (not shown). Both signals then appear to depend only on intracellular Ca^{2+} and to be triggered by a mechanism involving a voltage sensor similar to that described for skeletal muscle E-C coupling.

A different type of image appears in myotubes treated first with the SR Ca^{2+} channel blocker ryanodine (5–25 μM) and then exposed to a K^+ stimulus. In 12 independent experiments, after 15–30 min of incubation with ryanodine in Ca^{2+}-free solutions, the fast Ca^{2+} signal was no longer apparent. One sequence can be seen (Fig.

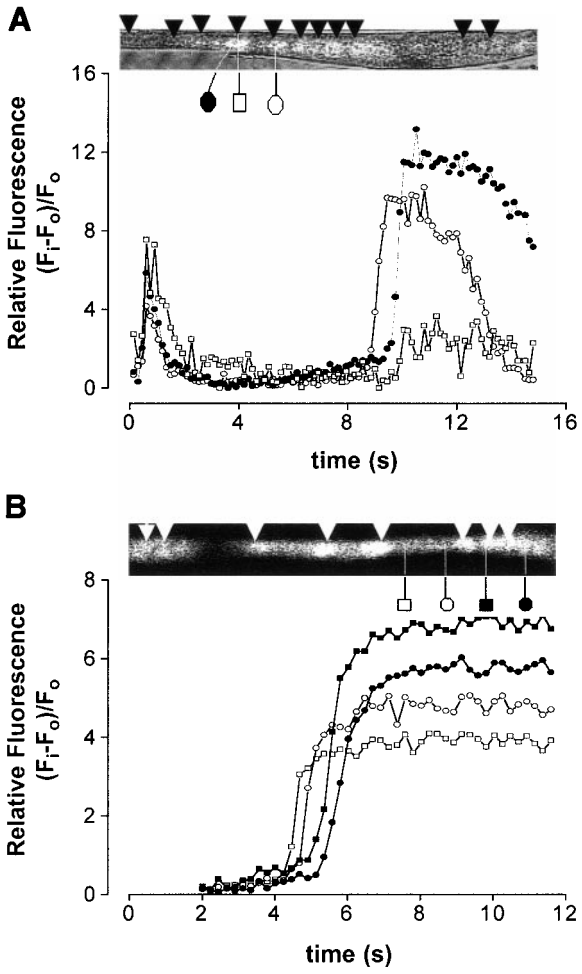

Fig. 7. Relative fluorescence change [ratio of fluorescence difference, stimulated − basal ($F_i - F_o$), to basal value (F_o)] as a function of time for 2 different myotubes. *A*: myotube, a portion of which is shown also in Fig. 5, is depicted in *inset* as transmitted light image superimposed onto fluorescence image taken at 10 s. A continuous train of nuclei (some indicated by arrowheads) is visible throughout entire length of myotube (354 μm). Regions of equivalent area are designated in spots indicated by lines: 2 spots correspond to location of cell nuclei (octagons), and 1 spot (□) corresponds to cytoplasm located next to nuclei and near plasma membrane. Relative fluorescence was calculated for each image in sequence. Fast Ca^{2+} signal and slow components were seen in this cell. *B*: same as *A*, except myotube shown in Fig. 6 (fluorescence image at 10 s) is indicated in *inset*. Two pairs of identical areas separated by same distance (34 μm) were chosen: one (open symbols) in a region devoid of active nuclei and one (filled symbols) in a region where several nuclei can be spotted together. Only slow Ca^{2+} signals were evident in this experiment.

8, *left*), where the first 2 s after high-K^+ perifusion are shown in images taken every 400 ms. No changes in fluorescence were apparent until many seconds later (see *bottom* fluorescence image taken after 24 s). The rise in fluorescence in a different ryanodine-treated myotube is shown in Fig. 8, *right*. Several seconds after the K^+ increase, the central part of the myotube became clearly fluorescent, but the propagation of the signal was no longer that of a slow wave. It was, rather, a sudden (or very quickly propagated) increase in fluorescence after a delay. Most of the fluorescence appears concentrated within the cell nuclei (Fig. 8, *right*). This type of nonpropagated, delayed Ca^{2+} rise was seen in 8 of 12 myotubes treated with ryanodine. Activation of ryanodine-sensitive channels, although not necessary for producing the delayed Ca^{2+} signals, appears to be needed for their propagation.

DISCUSSION

Ca^{2+} release in skeletal muscle is generally detected as a fast process mediated by dihydropyridine receptors (DHPR) in the T-tubule membrane and RyR in the SR (28). We provide evidence for another, second transient of $[Ca^{2+}]_i$ in cultured skeletal muscle cells. Furthermore, our evidence suggests the possible involvement of IP_3R, located in the cytoplasmic and nuclear envelope regions, in the generation of this second transient.

In studying depolarization of cultured skeletal muscle cells in response to high external K^+, we see evidence for at least two identifiable Ca^{2+} signals and at least two Ca^{2+} release systems. The two signals are the fast and slow waves; the two release systems are the RyR, associated with the fast wave, and the IP_3R, associated with the slow wave.

In fast-twitch skeletal muscle, elevated external K^+ concentration elicits a depolarization of the sarcolemma and a rise in tension followed by relaxation along an initial plateau phase and a subsequent phase of rapid relaxation. Although membrane depolarization persists in high external K^+ concentration, the fast, transient release of Ca^{2+} during the high external K^+ contracture probably reflects the physiological E-C coupling mechanism (21). In contrast, the slow Ca^{2+} signals we see in myotubes are not associated with contraction. We may conclude then that, during the slow wave, Ca^{2+} concentration in the myofibril region does not reach levels necessary for contraction; our experiments with fura 2-loaded myotubes do indeed show relatively low Ca^{2+} concentrations during the slow wave and support this conclusion. Slow waves, similar to those described here, were seen by Flucher and Andrews (12) in chicken myotubes exposed to caffeine, although they reported contraction in association with slow Ca^{2+} waves under those conditions. Complex Ca^{2+} signals in myotubes have also been reported by researchers using indo 1 as the Ca^{2+}-sensitive dye (10, 21). The kinetics of such signals could be resolved into two components: a fast and larger component, lasting a few seconds, and a slower component, lasting >30 s. The procedure used to measure those signals (light integration by a photomultiplier tube) does not allow space discrimination, since recorded signals integrate light coming from a slow propagating wave that spans only part of the cell volume at any time. The slow signals can fuse with the fast signal (21) or show a clearer time separation (10), probably depending on the geometry of the system.

We were able to show that fluorescence heterogeneity, observed during slow waves, corresponds to two separate processes: a more rapid increase in fluorescence (the slow-rapid wave) that propagates through nuclei and cytosol regions and a slower component (the slow-slow wave) seen only in the nuclear region. Nei-

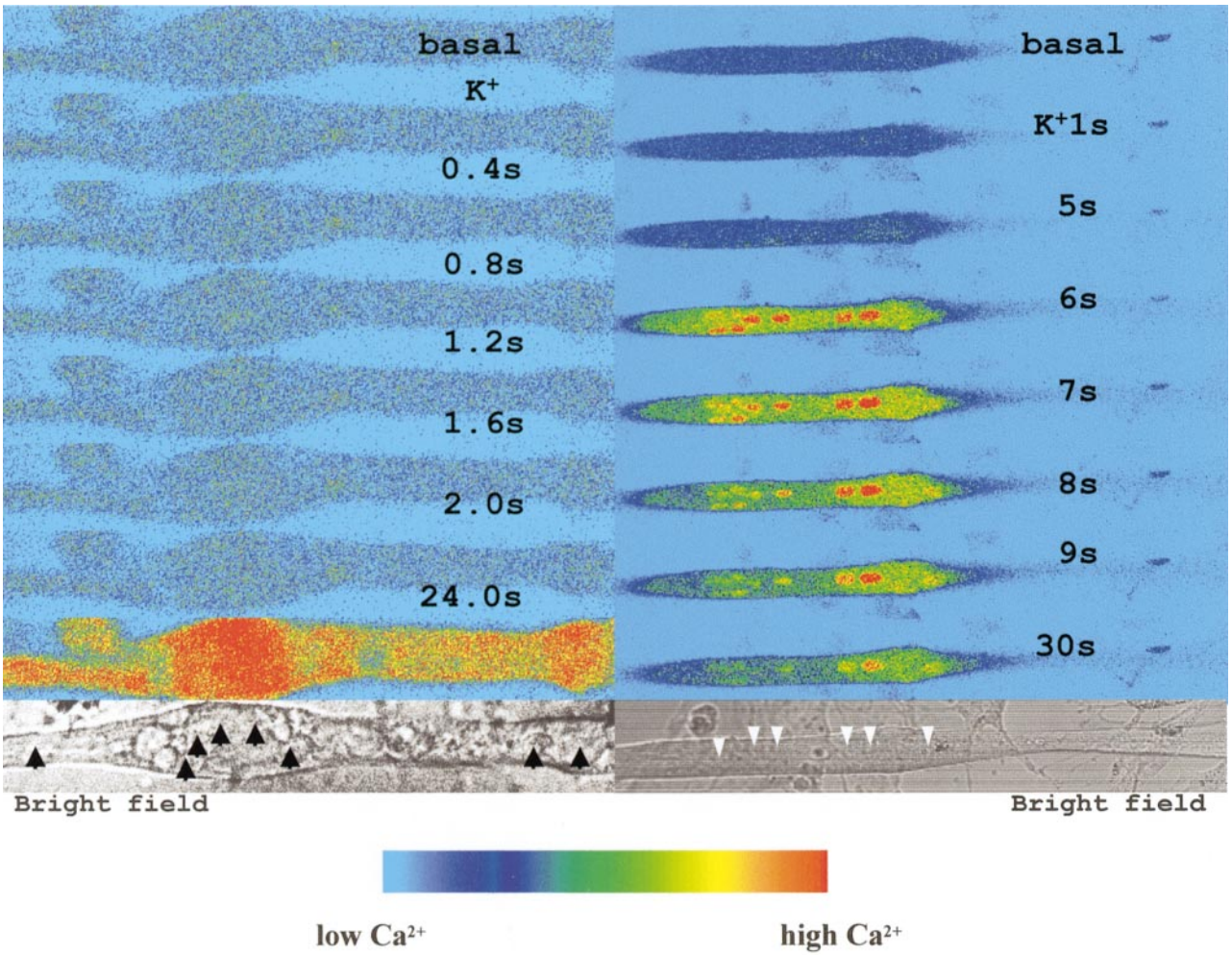

Fig. 8. Effect of ryanodine treatments on fast and slow waves. Arrowheads, nuclei. *Left*: a set of images taken every 400 ms in a myotube incubated for 30 min with 20 μM ryanodine. No fast signal is apparent; a delayed slow signal appears by 24 s. *Right*: a set of images in a myotube incubated for 20 min with 10 μM ryanodine. Fast Ca^{2+} signal is absent. After several seconds, central part of myotube became clearly fluorescent, but propagation of signal was not apparent. Most of fluorescence appears concentrated within cell nuclei. Total length of myotube segment is 208 μm.

ther dye inhomogeneity nor differences in the Ca^{2+}-buffering capacity could explain these phenomena; a possible explanation might be that Ca^{2+} is released from the nuclear envelope or perinuclear regions in response to the cytosolic slow-rapid wave. Measurements reported previously using indo 1 in these cells allowed an estimation of the total rise in $[Ca^{2+}]_i$ on K^+ stimulation; values ranged from ~100 nM in resting conditions to >400 nM after K^+ perifusion (21). This value corresponds kinetically to the fast Ca^{2+} signal, and the fura 2 experiments agree with that value. We have no measurement that corresponds to the slow wave.

The fact that the cell does not contract during the slow wave indicates that $[Ca^{2+}]_i$ remains low and that the high fluorescence spots we see must be highly compartmentalized in the nuclear region. Interestingly, in the presence of ryanodine, we were able to drastically alter the cytosolic propagation while preserving the slow Ca^{2+} rise, indicating that a ryanodine-sensitive Ca^{2+} pool may be involved in the mechanism of propagation through the cytosol. Cytosolic waves with variable propagation speed have been described in cardiac myocytes (38), and our cytosolic propagation shows similar features, the main difference being the much more slowly propagated nuclear component, a phenomenon that can only be imaged in multinucleated cells.

Ca^{2+} release channels have been shown to be present in a large variety of cells and can be grouped into two families: RyR and IP_3R (for review see Ref. 14). Only a function for RyR has been determined in skeletal muscle and, despite important evidence for the presence of inositol phosphate metabolism and IP_3R in skeletal muscle, their role remains elusive. The kinetics of increase in IP_3 concentration shown here are compatible with IP_3 being the Ca^{2+} release factor for the slow Ca^{2+} signals. It would be interesting to study the early (<4 s) part of the curve in detail, since it seems to be composed of two phases, possibly indicating two different processes for IP_3 production. An increase in the mass of IP_3 after cholinergic stimulation of these

cells has been described by us (32). In fact, in that work we show that carbachol (a cholinergic agonist) elicits a biphasic IP_3 increase much like that shown in Fig. 3. This increase is compatible with an early response to membrane depolarization mediated by nicotinic receptors; muscarine elicited a slower response. Membrane potential depolarization may then be the event that triggers an IP_3 increase and the subsequent slow Ca^{2+} wave.

Muscle tension development induced by IP_3 has been a highly controversial subject (29). It is conceivable that Ca^{2+} released from the nuclear envelope or from neighboring structures could be enough to elicit some contraction under certain special experimental conditions but not necessarily under normal, physiological conditions. It is also conceivable that IP_3-sensitive Ca^{2+} channels reported in SR vesicles (36, 37) could come from perinuclear or compartmentalized SR. Nevertheless, our results do not rule out additional roles for IP_3 in muscle cells, E-C coupling included, since we have seen immunostaining for IP_3 receptors in muscle fiber striations. The role for such receptors remains to be studied.

The presence of functional muscarinic receptors in cultured myotubes (32) and the fact that IP_3 increases transiently in myotubes on K^+ depolarization suggest that V_m (via voltage sensors) and membrane ligand receptors can be linked to IP_3 production. DHPR may be involved in these signals as voltage sensors, since slow Ca^{2+} signals can be blocked by nifedipine, a specific antagonist of DHPR (21).

Direct evidence for the involvement of IP_3 receptors in slow Ca^{2+} transients comes from a collaborative work using marine sponge toxins able to block IP_3-mediated responses. Such compounds were able to block the slow Ca^{2+} wave without altering the fast transient (unpublished observations).

The apparently different intracellular distributions of receptors, RyR in the SR membranes and IP_3R (at least in some developmental stages), concentrated in membranes associated with the nuclei point to the presence of two separate Ca^{2+} release systems. We believe that the staining of the nuclear envelope region with the affinity-purified type 1 IP_3R supports the finding that the IP_3R binding is enriched in nuclear fractions. The specific subcellular localization of the immunocytological IP_3R "striations" in mature myotubes is under study. The antibody used in this study has detected IP_3R in microsomes prepared from vascular smooth muscle (Affinity Bioreagents information) and may therefore be the form found by Chadwick et al. (9) in smooth muscle. It is possible that skeletal muscle also contains this form. From the control immunocytological experiments performed in the present study, it is clear that the labeling of the envelope region is specific for the IP_3R, since the internal nuclear structures also stain with preimmune serum and with peptide adsorbed affinity-purified antibody. This nuclear envelope labeling does not appear to us to represent perinuclear Golgi label and thus be IP_3R "on route" to its destination.

We can speculate that the slow waves elicited by K^+ depolarization and associated with increased nucleoplasmic Ca^{2+} may have an important role in the regulation of gene expression during muscle development. If such signals can be demonstrated in adult skeletal muscle, they could be related to functions as important as the phenomenon of exercise adaptation (2, 31). They could also have a role in muscle hypertrophy in human muscular dystrophy. We have shown that dystrophic muscle cell lines (human and mouse) show a two- to threefold increase in basal levels of IP_3, and the number of IP_3R is also significantly higher in dystrophic than in normal cells (24). The process of excitation-transduction coupling via the IP_3 cascade may be relevant then for developing muscle and for gene expression associated with exercise and/or disease.

The complex pattern of signal pathways from plasma membrane to nucleus that begins to arise opens interesting possibilities for future study of new, Ca^{2+}-mediated processes in muscle cells.

We are grateful for the able assistance of Soledad Tascón in cell culture and Manuel Estrada, Steven O'Neil, and Tomás Pérez in image analysis.

This work was financed by the Muscular Dystrophy Association (E. Jaimovich and J. A. Powell), the Blakeslee Fund of Smith College (J. A. Powell), the European Economic Community and Fondo Nacional de Ciencia y Tecnología Grant 8980010. The institutional support to Centro de Estudios Científicos de Santiago of Fuerza Aerea de Chile, Municipalidad de Las Condes, and a group of Chilean companies (AFP Provida, CGE, Codelco, COPEC, Empresas CMPC, Gener, Minerva Collahuasi, Minerva Escondida, Novagas, Business Design Associates, and Xerox Chile) is also recognized.

Address for reprint requests and other correspondence: E. Jaimovich, Casilla 70005, Santiago 6530499, Chile (E-mail: ejaimovi @machi.med.uchile.cl).

Received 12 July 1999; accepted in final form 17 December 1999.

REFERENCES

1. **Berridge MJ.** Inositol trisphosphate and calcium signalling. *Nature* 361: 315–325, 1993.
2. **Booth F and Thomason D.** Molecular and cellular adaptation of muscle in response to exercise: perspectives of various models. *Physiol Rev* 71: 541–585, 1991.
3. **Bredt DS, Mourey RJ, and Snyder SH.** A simple sensitive and specific radioreceptor assay for inositol 1,4,5-trisphosphate in biological tissues. *Biochem Biophys Res Commun* 59: 976–982, 1989.
4. **Burgoyne R and Cheek T.** Locating intracellular calcium stores. *Trends Biochem Sci* 16: 319–320, 1991.
5. **Cahill M, Janknecht R, and Nordheim A.** Signalling pathways: jack of all cascades. *Curr Biol* 6: 16–19, 1996.
6. **Carrasco MA and Figueroa S.** Inositol 1,4,5-trisphosphate activity in frog skeletal muscle. *Comp Biochem Physiol B Biochem Mol Biol* 110: 747–753, 1995.
7. **Carrasco MA, Marambio P, and Jaimovich E.** Changes in IP_3 metabolism during skeletal muscle development in vivo and in vitro. *Comp Biochem Physiol B Biochem Mol Biol* 116: 173–181, 1997.
8. **Carrasco MA, Sierralta J, and Hidalgo C.** Phospholipase C activity in membranes and a soluble fraction isolated from frog skeletal muscle. *Biochim Biophys Acta* 1152: 44–48, 1993.
9. **Chadwick C, Saito A, and Fleischer S.** Isolation and characterization of the inositol trisphosphate receptor from smooth muscle. *Proc Natl Acad Sci USA* 87: 2132–2136, 1990.
10. **Cognard C, Constantin B, Rivet-Bastide M, and Raymond G.** Intracellular calcium transients induced by different kinds of

stimulus during myogenesis of rat skeletal muscle cells studied by laser cytofluorimetry with indo-1. *Cell Calcium* 14: 333–348, 1993.
11. **Downes CP and Michell RH.** The polyphosphoinositide phosphodiesterase of erythrocyte membrane. *Biochem J* 198: 133–140, 1981.
12. **Flucher B and Andrews S.** Characterization of spontaneous and action potential-induced calcium transients in developing myotubes in vitro. *Cell Motil Cytoskeleton* 25: 143–157, 1993.
13. **Flucher BE, Phillips JL, and Powell JA.** Dihydropyridine α-receptor subunits in normal and dysgenic muscle in vitro: expression of the α_1 is required for the proper targeting and distribution of α_2. *J Cell Biol* 115: 1345–1356, 1991.
14. **Furuichi T, Kohda K, Miyawaki A, and Mikoshiba K.** Intracellular channels. *Curr Opin Neurobiol* 4: 294–303, 1994.
15. **Furuichi T, Yoshikawa S, Miyawaki A, Wada K, Maeda N, and Mikoshiba K.** Primary structure and functional expression of the inositol 1,4,5-trisphosphate-binding protein P400. *Nature* 342: 32–38, 1989.
16. **Ginty D.** Calcium regulation of gene expression: isn't that spatial? *Neuron* 18: 183–186, 1997.
17. **Hidalgo J, Niemeyer MI, and Jaimovich E.** Voltage control of calcium transients elicited by caffeine and tetracaine in cultured rat muscle cells. *Cell Calcium* 18: 140–154, 1995.
18. **Humbert JP, Matter N, Artault JC, Köppler P, and Malviya AN.** Inositol 1,4,5-trisphosphate receptor is located to the inner nuclear membrane vindicating regulation of nuclear calcium signalling by inositol 1,4,5-trisphosphate. *J Biol Chem* 271: 478–485, 1996.
19. **Jaimovich E.** Chemical transmission at the triad: $InsP_3$? *J Muscle Res Cell Motil* 12: 316–320, 1991.
20. **Jaimovich E, Donoso P, Liberona JL, and Hidalgo C.** Ion pathways in transverse tubules. Quantification of receptors in membranes isolated from frog and rabbit skeletal muscle. *Biochim Biophys Acta* 855: 89–98, 1986.
21. **Jaimovich E and Rojas E.** Intracellular Ca^{2+} transients induced by high external K^+ and tetracaine in cultured rat myotubes. *Cell Calcium* 15: 356–368, 1994.
22. **Karin M and Hunter T.** Transcriptional control by protein phosphorylation signal transmission from the cell surface to the nucleus. *Curr Biol* 5: 747–757, 1995.
23. **Liberona JL, Caviedes P, Tascón S, Hidalgo J, Giglio JR, Sampaio SV, Caviedes R, and Jaimovich E.** Expression of ion channels during differentiation of a human skeletal muscle cell line. *J Muscle Res Cell Motil* 18: 587–598, 1997.
24. **Liberona JL, Powell JA, Shenoi S, Petherbridge L, Caviedes R, and Jaimovich E.** Differences in both inositol 1,4,5-trisphosphate mass and inositol 1,4,5-trisphosphate receptors between normal and dystrophic skeletal muscle cell lines. *Muscle Nerve* 21: 902–909, 1998.
25. **Lui PPY, Kong SK, Fung KP, and Lee CY.** The rise of nuclear and cytosolic Ca^{2+} can be uncoupled in HeLa cells. *Pflügers Arch* 436: 371–376, 1998.
26. **Malviya AN and Rogue PJ.** "Tell me where is calcium bred": clarifying the roles of nuclear calcium. *Cell* 92: 17–23, 1998.
27. **Malviya AN, Rogue P, and Vincendon G.** Stereospecific inositol 1,4,5-trisphosphate binding to isolated rat liver nuclei: evidence for inositol trisphosphate receptor-mediated calcium release from the nucleus. *Proc Natl Acad Sci USA* 87: 9270–9274, 1994.
28. **Melzer W, Herrmann-Frank A, and Luttgau HC.** The role of Ca^{2+} ions in excitation-contraction coupling of skeletal muscle fibres. *Biochim Biophys Acta* 1241: 59–116, 1995.
29. **Posterino GS and Lamb GD.** Investigation of the effect of inositol trisphosphate in skinned skeletal muscle fibres with functional excitation-contraction coupling. *J Muscle Res Cell Motil* 19: 67–74, 1998.
30. **Powell JA, Petherbridge L, and Flucher BF.** Formation of triads without the dihydropyridine receptor α-subunits in cell lines from dysgenic skeletal muscle. *J Cell Biol* 134: 375–387, 1996.
31. **Puntschart A, Wey E, Jostarndt K, Vogt M, Wittwer M, Widmer Hoppeler HR, and Billeter R.** Expression of *fos* and *jun* genes in human skeletal muscle after exercise. *Am J Physiol Cell Physiol* 274: C129–C137, 1998.
32. **Reyes R and Jaimovich E.** Functional muscarinic receptors in cultured skeletal muscle. *Arch Biochem Biophys* 331: 41–47, 1996.
33. **Rousseau E, Michaud C, Lefebvre D, Proteau S, and Decrouy A.** Reconstitution of ionic channels from inner and outer membranes of mammalian cardiac nuclei. *Biophys J* 70: 703–714, 1996.
34. **Scherer NM, Toro M, Entman ML, and Birnbaumer L.** G-protein distribution in canine cardiac sarcoplasmic reticulum and sarcolemma. Comparison to rabbit skeletal muscle membranes and to brain and erythrocyte G-proteins. *Arch Biochem Biophys* 259: 431–440, 1987.
35. **Stehno-Bitel L, Luckhoff A, and Clapham DE.** Calcium release from the nucleus by $InsP_3$. *Neuron* 14: 163–167, 1995.
36. **Suarez-Isla BA, Irribarra V, Oberhauser A, Larralde L, Bull R, Hidalgo C, and Jaimovich E.** Inositol 1,4,5 trisphosphate activates a calcium channel in isolated sarcoplasmic reticulum membranes. *Biophys J* 54: 737–741, 1988.
37. **Volpe P, Di Virgilio F, Pozzan T, and Salviati G.** Role of inositol 1,4,5-trisphosphate in excitation-contraction coupling in skeletal muscle. *FEBS Lett* 197: 1–4, 1985.
38. **Wussling MHP and Salz H.** Nonlinear propagation of spherical calcium waves in rat cardiac myocytes. *Biophys J* 70: 1144–1153, 1996.